

Article

High-Pressure Aging of Asymmetric Torlon[®] Hollow Fibers for Helium Separation from Natural Gas

George Dibrov^{1,*}, Mikhail Ivanov¹, Mikhail Semyashkin¹, Vladislav Sudin² and Georgy Kagrananov¹

¹ Dmitry Mendeleev University of Chemical Technology of Russia, 125047 Moscow, Russia; mihail-ivanov@yandex.ru (M.I.); mixailsem@rambler.ru (M.S.); kadri@muctr.ru (G.K.)

² Baikov Institute of Metallurgy and Materials Science, Russian Academy of Sciences, 125047 Moscow, Russia; sudin.vlad@gmail.com

* Correspondence: George.dibrov@gmail.com; Tel.: +7-915-2119477

Received: 2 September 2018; Accepted: 23 October 2018; Published: 25 October 2018



Abstract: Membrane separation for helium extraction from natural gas gained increased interest recently. Several vendors offer membrane elements for helium extraction, although data on their performance and operating experience are unpublished. The aim of this work was to obtain and study the separation performance of asymmetric hollow-fiber membrane element from commercial polyamide-imide Torlon[®], in conditions close to the industrial process of helium extraction from natural gas. A membrane element with an active area of 0.177 m², a helium permeance of 100 l(STP)/(m²·h·bar), and a selectivity $\alpha(\text{He}/\text{CH}_4) = 340$ was produced. This corresponds to a selective layer thickness of 82.3 nm, which was confirmed by SEM and resistance model calculations. The obtained membrane element was employed to decrease the concentration of helium in its binary mixture with methane from 0.4% to 0.05%. A relationship of separation characteristics from transmembrane pressure is also presented. At 70 bar and a stage cut of 2.7%, the feed flow rate was 0.16 m³(STP)/h, which yielded a helium permeate concentration of 14.7%. At 80 bar, a decrease in permeance to 60 l(STP)/(m²·h·bar) and in selectivity to 240 was observed. It was shown that the main reason for aging was the increased support resistance, due to a partial compaction of pores with a radius of less than 15 nm.

Keywords: polymeric hollow-fiber membranes; helium; gas separation; aging

1. Introduction

Helium is a finite, nonrenewable, unique, and precious resource that can be extracted from only a few natural-gas fields around the globe [1]. Because of the delicate balance between helium availability and increasing demand, its recovery and conservation are imperative.

Currently, helium is extracted using cryogenic distillation. However, given its energy intensiveness, capital, and operational costs, membrane helium separation is a viable alternative [2]. For the first time, membranes from quartz were applied for helium extraction in 1958 [3], while polymeric membranes were used in 1965 [4]. In 1973, a four-stage membrane pilot plant was constructed that could process 3500 m³(STP)/h of gas containing 0.05% helium. The membrane unit produced a helium concentration of 72 to 90%. Further on-site processing produced a final helium purity of 99.997% [5]. At the moment, companies such as Ube, Air Liquid, Evonik, Generon, and Tecon MT manufacture hollow-fiber membrane elements (MEs), while UOP manufactures spiral-wound MEs, capable of extracting helium from natural gas.

For helium separation, the necessity for ME operation at elevated pressure (>40 bar) and temperature is stipulated by both the demands of the pipeline transport system and the enhanced

separation performance of ME in such conditions. On this basis, membrane materials must possess high values of tensile and yield strength.

The most important membrane separation characteristics are permeance and selectivity. Permeance (P/l) defines the required membrane area, i.e., the size of the unit and, hence, a substantial portion of the capital cost and, correspondingly, of depreciation [6]. This parameter is calculated using the following formula:

$$\frac{P}{l} = \frac{V}{\tau S \Delta p'} \quad (1)$$

where P is the permeability, l is the selective layer thickness, V/τ is the volumetric flow rate, S is the membrane area, and $\Delta p'$ is the transmembrane pressure. Permeance is measured in $l(\text{STP})/(\text{m}^2 \cdot \text{h} \cdot \text{bar})$, equivalent to 0.3703 gas permeation units (GPU) or $1.239 \times 10^{-10} \text{ mol}/(\text{m}^2 \cdot \text{s} \cdot \text{Pa})$. Dimensionless membrane selectivity determines the power consumption by the compressor equipment at the entrance of the ME, i.e., a significant portion of operating costs. Selectivity is calculated as a ratio of permeances of fast permeating species (A) relative to slow permeating species (B):

$$\alpha(A/B) = \frac{P_A/l}{P_B/l} \quad (2)$$

Despite the variety of commercial companies which produce MEs for helium extraction from natural gas, data on polymer chemical structures being used, and membrane separation performance are scarcely presented in the literature [7,8]. Vigorous work was conducted in the field of synthesis of new polymer materials with promising helium separation characteristics [9,10], although few of them are known to be processed into asymmetric hollow fibers.

One such polymer which could be employed for membrane helium extraction is polyamide-imide (PAI) with the commercial name Torlon[®]. It has high tensile strength in a broad temperature range, high permeability, and high helium/methane selectivity: $P(\text{He}) = 4.4 \text{ Barrer}$ ($1 \text{ Barrer} = 3.347 \times 10^{-16} \text{ (mol} \cdot \text{m)}/(\text{m}^2 \cdot \text{s} \cdot \text{Pa})$), $\alpha(\text{He}/\text{CH}_4) = 490$ [11]. A technique is described in Reference [11] for obtaining asymmetric hollow fibers from Torlon[®], capable of withstanding nitrogen pressure up to 138 bar. The helium permeance of these membranes was $20 \text{ l}/(\text{m}^2 \cdot \text{h} \cdot \text{bar})$, $\alpha(\text{He}/\text{CH}_4) = 320$, which corresponds to a selective layer thickness of $0.41 \mu\text{m}$. Peng et al. [12–14] obtained asymmetric hollow fibers from Torlon[®] with an ultra-thin dense layer of around 54 nm and excellent O_2/N_2 selectivity, although He/ CH_4 separation properties were not studied.

An important phenomenon, which gained attention in recent papers, is the decrease in membrane permeance over time, also called “aging” [15,16]. This effect becomes even more pronounced for thin films, at higher temperatures and pressures [17], which is important for natural-gas treatment. Aging was studied on free-standing films [18,19] and composite membranes [17,20,21]. To the best of our knowledge, the aging of asymmetric hollow fibers, obtained using the phase-inversion technique, is yet to be studied.

The purpose of this work was to investigate the influence of spinning process parameters on the helium separation characteristics of asymmetric hollow fibers from Torlon[®] PAI. Their behavior was studied in terms of separation performance and aging as a function of transmembrane pressure at conditions close to industrial membrane-based applications for helium recovery.

2. Materials and Methods

2.1. Materials

Torlon[®] 4000T powder was supplied by Solvay polymers. Pure gases of helium (99.995% vol.) and methane (99.99% vol.), as well as a gas mixture containing 0.4% vol. helium and 99.6% vol. methane, was provided by the Moscow Gas Processing Plant (MGPZ). *N*-methyl-2-pyrrolidone (NMP), tetrahydrofuran (THF), and hexane, all reagent grade, were purchased from Khimmed. Ethanol

(EtOH, 95%) and reverse-osmosis water with a specific conductivity of no more than $0.06 \mu\text{S}/\text{cm}$ were also used. Sylgard 184 (polydimethylsiloxane (PDMS)) was produced by Dow Corning.

2.2. Asymmetric Hollow-Fiber Spinning and Characterization

Asymmetric hollow-fiber membranes were made using the “dry-wet” spinning technique. The dope (polymeric solution) contained the polymer; NMP was chosen as a good solvent; THF was chosen as a moderate solvent with high volatility, to enhance the skin-layer formation; and ethanol was chosen as a non-solvent due to its good pore-forming properties [22]. For asymmetric hollow fibers to possess good mechanical properties, the polymer content was chosen to be 30% wt. The composition of other additives was determined using the cloud-point technique, by titrating non-solvent into a solution containing the polymer and solvents until the appearance of turbidity (phase separation).

The resulting solution contained 30% wt. polymer, 53% wt. NMP, 10% wt. THF, and 7% wt. ethanol. To obtain the dope solution, the polymer was added to NMP at 50°C , under constant stirring, followed by the addition of THF and ethanol. To prevent the evaporation of volatile solvents (THF and ethanol), a stirrer bearing with a dynamic double seal was employed, and the total weight of the solution was controlled. Afterward, the dope was kept undisturbed at that temperature overnight for degassing.

The schematic of the set-up for asymmetric hollow-fiber spinning is presented in Figure 1 and it was described in detail in References [22–24]. The dope solution tank was equipped with a thermal jacket and a gear pump. A spinneret with a dope orifice outer diameter of 0.8 mm and an inner diameter of 0.23 mm was employed. The dope solution flow rate was kept constant at 1.2 g/min. Water at 50°C was used as a bore fluid at a constant flow rate of 0.2 g/min. The temperature of water in the coagulation bath was 27°C or 40°C . Water at room temperature was used in washing baths.

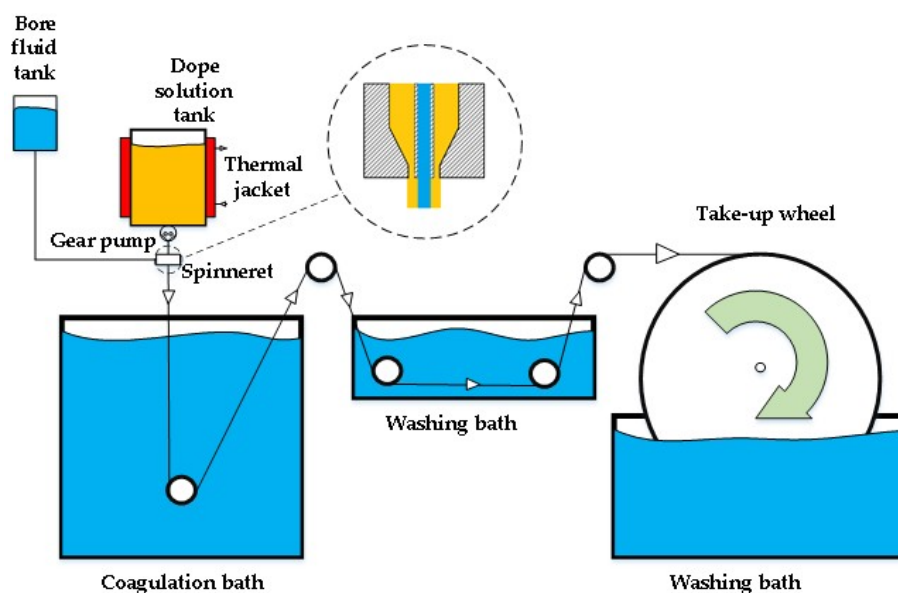


Figure 1. Hollow-fiber membrane-spinning apparatus.

The resulting asymmetric membranes were kept in water for 48 h to remove the residual solvent, followed by sequential solvent substitutions to prevent pore collapse. The membrane was placed for 24 h in ethanol, then for 8 h in hexane, and finally dried in a vacuum (76 mmHg) for 12 h.

Membranes were treated with 0.2% wt. PDMS solution in hexane. Treatment of the asymmetric membranes with highly permeable rubbery PDMS has been used since the first gas separation asymmetric hollow fibers were reported [25]. Such a post-treatment procedure was necessary to plug the defects in the thin dense skin layer. It is worth noting that new rubbery polymer materials for gas separation have appeared since then [26,27].

Afterward, membranes were dried in ambient air for 1–2 h and annealed in air at 60 °C for 3–4 h. This was performed to fully cross-link PDMS, and to stabilize the geometrical and separation characteristics of the membrane because physical aging is known to occur faster at higher temperatures [17].

Pure helium and methane permeances were determined using the constant-pressure variable-volume technique described elsewhere [17], at transmembrane pressure $\Delta p = 2$ bar, $T = 35$ °C, with a shell-side feed. Errors in gas permeance measurements did not exceed 5%, while those for selectivity calculations did not exceed 10%.

To measure the internal and external diameters of hollow fibers, a Levenhuk 40L NG microscope equipped with a C310 NG 3M digital camera was used. Samples were held for 0.5–1 h in ethanol with subsequent freeze-fracturing in liquid nitrogen. Deviations in fiber diameters did not exceed 4%.

Cross-sections of freeze-fractured asymmetric hollow fibers were studied using scanning electron microscopy (SEM). A high-resolution scanning electron microscope Supra 50 VP LEO (Carl Zeiss SMT Ltd., Oberkochen, Germany) was used at an accelerating voltage of 4.5 kV and an aperture of 30 μm . To process and analyze the SEM micrographs, the Gwyddion software (Czech Metrology Institute, Brno, Czech Republic) was employed.

To measure the porosity, a gravimetric method was used. A representative number of fibers with equal length were weighed on scales, and the porosity (ϵ) was calculated using Equation (3).

$$\epsilon = \frac{\rho_p - \rho_g}{\rho_p} = \frac{\rho_p - m/V_g}{\rho_p}, \quad (3)$$

where ρ_p and ρ_g are the pycnometric (1.42 g/cm³) and geometric densities, m is the weight of the fibers, and V_g is the geometric volume, calculated using optical microscopy. Such a method is not the most accurate to determine the porosity; however, it fits to compare different samples. Nitrogen adsorption measurements were performed using a Gemini VII 2390t (Micromeritics Instrument Corp., Norcross, GA, USA), pore size distribution was calculated according to the Barrett–Joyner–Halenda (BJH) method.

2.3. Membrane Element Preparation

To measure gas separation characteristics of the obtained hollow fibers and their relationship with transmembrane pressure, the membrane element (module) was assembled using Hy-Lok fittings and 12 \times 1 tubes (stainless steel S316/316L). To this effect, 200 fibers with epoxy-sealed ends were fixed inside the module assembly. A syringe with epoxy resin was attached to one end and the assembly was centrifuged at 300 rpm for 8–12 h to better distribute the highly viscous epoxy resin between the fibers and to prevent the capillary uprise. The end of the module, attached to the tube with the epoxy resin, was cut with a sharp knife to open the lumen side of hollow fibers. The other sealed end was unattached and lay freely inside the tube. The active length of the ME was 0.67 m, with a potted length of 0.15 m, and an active membrane area of 0.177 m².

The membrane element was treated with 0.2% wt. PDMS solution in hexane in the same manner as the hollow fibers. After draining the solution, the membrane element was vented with air for 2–4 h and annealed at 60 °C in air for 2–4 h.

2.4. Mixed-Gas Test

For industrial applications, membrane elements have to undergo endurance tests, which reveal how separation parameters change over time during natural-gas treatment. To imitate natural helium-containing gas, a model gas was used, comprising 0.4% helium and 99.6% methane. The experimental set-up for the mixed-gas tests of the ME is presented in Figure 2. The gas was pressurized to the shell side of ME. Its pressure was controlled using a membrane pressure regulator on the inlet, and the flow rate was controlled using a needle flow regulator on the outlet of the ME.

The flow rate of retentate (non-permeated gas stream) and permeate (permeated gas stream) was measured using a bubble flow meter, while the feed gas flow rate was calculated as a sum of the permeate and retentate. The concentration of helium in the permeate and retentate was measured using a portable gas chromatograph AHT-TI (Mikroprocessonnye Tekhnologii, Moscow, Russia) equipped with a thermal conductivity sensor and a Porapak™ column, with air as the carrier gas. The experimental error for the mass balance calculation did not exceed 5%.

Conditions of the experiment were chosen to simulate a real gas separation application. The temperature was kept at 35 °C, and the pressure was elevated up to 80 bar. The stage cut (θ), defined as a dimensionless ratio of permeate to feed-gas flow rates, was adjusted to produce a retentate flow with a 0.05% concentration of helium. This value was chosen because, according to Russian standards (GOST R 535212009), gas is considered helium-rich if the helium concentration exceeds 0.05% [6].

To investigate the influence of transmembrane pressure, it was increased and decreased step-wise incrementally. Each transmembrane pressure was maintained until the results of three consecutive measurements converged within the margin of error.

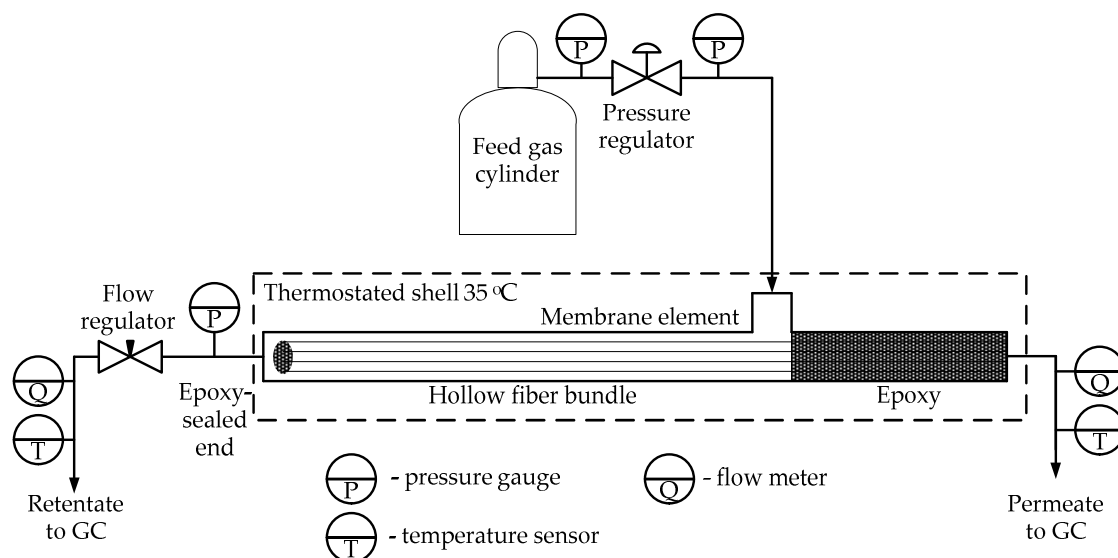


Figure 2. Experimental set-up for mixed-gas tests of the membrane element.

To calculate the permeance and selectivity, a counter-current mathematical model was employed, which involved the solution of a system of two differential linear equations using Euler's method. The algorithm is described elsewhere [28,29].

3. Results and Discussion

3.1. Hollow Fiber Spinning

The influence of spinning parameters, such as air-gap height, take-up speed (v), draw ratio, and temperature of the coagulation bath, on the geometrical and separation characteristics are presented in Table 1. At an air-gap height of 9 cm, hollow fibers were obtained with outer (OD) and internal (ID) diameters of 420 and 240 μm , respectively. The helium permeance value was determined as 105 l(STP)/($\text{m}^2 \cdot \text{h} \cdot \text{bar}$) at a selectivity of $\alpha(\text{He}/\text{CH}_4) = 360$.

Table 1. The influence of spinning parameters on the hollow fiber's geometrical and separation characteristics. OD—Outer diameter; ID—Internal diameter.

#	Air Gap, cm	v^1 , m/min	Draw Ratio	T^2 , °C	OD, μm	ID, μm	$P/l(\text{He})^3$	$\alpha(\text{He}/\text{CH}_4)$
1	9	7	2.7	40	420	240	105	360
2	3	7	2.7	40	420	240	106	345
3	9	9	3.5	40	370	220	100	320
4	9	7	2.7	27	420	240	63	260

¹ take-up speed; ² coagulation bath temperature; ³ in $\text{l}(\text{STP})/(\text{m}^2\cdot\text{h}\cdot\text{bar})$.

The value of selectivity was smaller than the intrinsic polymer properties [11], which can be explained by two reasons. Firstly, small defects are almost inevitably produced when one tries to minimize the selective layer thickness. These defects were plugged with PDMS, which has a significantly lower selectivity than PAI. Secondly, substructure resistance can cause a decrease in the selectivity [11]. The permeation mechanism in the substructure obeys the Knudsen or Hagen–Poiseuille models, which are considerably less selective than the solution–diffusion model in the case of PAI. Methane has a substantially lower transport substructure resistance due to a slower permeation rate through the selective layer. Therein, such resistance would decrease the permeation of “fast” helium compared to “slow” methane. This effect was described with resistance models by Henis and Tripodi [25]. The support resistance was also discussed in References [11,30–33] in relation to gas separation properties of hollow fibers.

In the case of support resistance, it is more correct to evaluate effective skin-layer thickness using “slow” gas permeance. From Table 1, line 1, it can be seen that methane permeance was $0.2917 \text{ l}(\text{STP})/(\text{m}^2\cdot\text{h}\cdot\text{bar})$. According to the polymer intrinsic properties reported in Reference [11], the methane permeance of a $1\text{-}\mu\text{m}$ -thick film is $0.0242 \text{ l}(\text{STP})/(\text{m}^2\cdot\text{h}\cdot\text{bar})$. Since membrane gas permeance is inversely proportional to the selective layer thickness, for the first regime, the effective skin-layer thickness derived from methane permeance was 83 nm.

The decrease in air-gap height affected neither the geometrical nor the separation characteristics of the membrane. With the increase in draw ratio, which is the ratio of linear velocities of the take-up wheel and polymer extrusion, the outer and inner diameters decreased. The decrease in selectivity can be explained by the growth in defect number, accompanying an increase in stretching tension.

The temperature of the coagulation bath, sometimes called a “quenching” bath, is also an important parameter which affects membrane separation characteristics. In this work, the decrease in coagulation bath temperature resulted in a decline in both permeance and selectivity. The cause of this decline can be explained by the reduction in interdiffusion coefficients between the polymeric solution and the coagulation bath during the phase inversion. In such conditions, the rates of solvent outflow from the hollow fiber to the coagulation bath, and water influx from the coagulation bath to the hollow fiber are slower. Apparently, a more densely packed support layer was obtained, which increased the support resistance and declined the selectivity and permeance. In Reference [34], raising the coagulation bath temperature while spinning 6FDA/6FDAM hollow fibers induced three-dimensional open-cell pore formation, which was confirmed by SEM. In Reference [35], a higher coagulation bath temperature resulted in increased porosity. It is likely that the decline in permeance in this work was also contributed by the thicker skin layer.

3.2. Scanning Electron and Optical Microscopy

For further experiments, hollow fibers obtained from the first regime were used. SEM (Figure 3a) and optical microscopy (Figure 3b) were employed to study the microstructure of the hollow fiber cross-section. The outer and inner diameters measured using both methods were in good agreement. “Macrovoids” were observed both on the outer and at the inner edges of the fiber. The sizes of these voids were $10 \mu\text{m}$ and $20\text{--}30 \mu\text{m}$, respectively. Because of the small size, these voids did not exert significant influence on the membrane mechanical properties. As shown later, the membrane was

capable of withstanding elevated pressures of up to 80 bar. For a further improvement of mechanical properties, macrovoids in the structure can be eliminated, which can be accomplished by increasing the dope viscosity [11,36] or through the proper adjustment of spinning parameters [37].

SEM microscopy allowed studying the selective skin-layer region of the hollow fiber (Figure 4a,b). Micrographs revealed that the structure in this region was composed of closely packed spherical polymer aggregates with sizes of 30–60 nm. A distinctive feature of the selective layer was the absence of any noticeable interspacing between these aggregates. In Figure 4b, the selective layer was partially peeled off due to freeze fracture and was lifted upward, which allowed the measuring of its thickness more carefully. The skin-layer thickness was roughly estimated as approximately 80 nm, which agrees well with the gas permeance test. Under the skin layer, a transition layer was observed with an interspacing of 5–15 nm between the aggregates (Figure 4a). The value of this transition layer thickness was roughly estimated as approximately 0.75 μm .

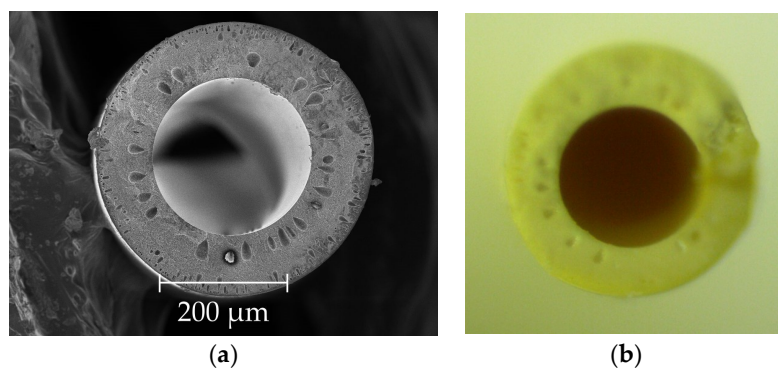


Figure 3. (a) SEM micrograph of the hollow fiber cross-section; (b) optical micrograph of the hollow fiber cross-section.

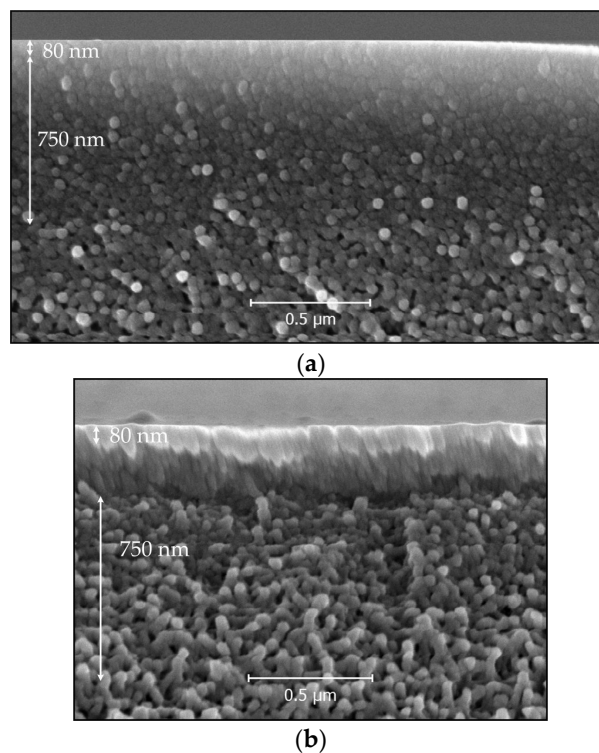


Figure 4. (a) SEM micrographs of hollow fiber cross-section with a close-up of the selective layer; (b) the selective layer is slightly peeled off.

The micrograph of the asymmetric membrane support layer is presented in Figure 5a. The average pore size was 0.2–0.4 μm , and its porosity was approximately 70%. The value of porosity obtained by SEM was in good agreement with the value determined gravimetrically (67%). The micrograph of the cross-section in the vicinity of the inner edge (Figure 5b) revealed another transition layer with a pore size of 40–80 nm.

The transition layers at the outer and inner edges of the fiber were obtained as a result of polymer concentration at the respective surfaces upon phase inversion. Firstly, they accounted for the observed macrovoids, because they reduced the rate of solvent outflow from the fiber [38]. Secondly, they accounted for substantial gas transport resistance, which caused the selectivity of the hollow fiber to be lower than its intrinsic properties.

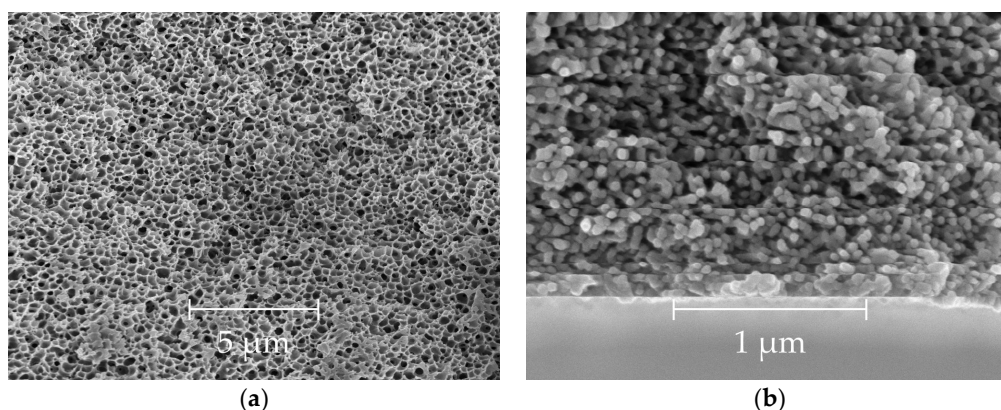


Figure 5. SEM micrographs of hollow fiber cross-section with close-ups of (a) the support layer, and (b) the inside layer.

3.3. Membrane-Element Mixed-Gas Test

The mixed-gas test was carried out to measure helium concentrations and the flow rates of permeate and retentate (material balance) for the obtained membrane element; afterward, helium permeance and selectivity were calculated using a counter-current mathematical model. In this test, the concentration of helium was reduced from 0.4% in the feed to 0.05% in the retentate. Relationships of permeance and selectivity $\alpha(\text{He}/\text{CH}_4)$ with transmembrane pressure are presented in Figure 6.

The initial test ME separation parameters were measured at a transmembrane pressure of 2 bar; the helium permeance was $100 \text{ l(STP)}/(\text{m}^2 \cdot \text{h} \cdot \text{bar})$ and the selectivity $\alpha(\text{He}/\text{CH}_4)$ was 340, which agrees well with the results obtained for the individual hollow fibers. A negligible deviation may be ascribed to the imperfection of the mathematical model, which does not take into consideration effects such as pressure build-up inside the lumen side of the hollow fiber, and other non-ideal effects [39].

With the incremental increase in transmembrane pressure up to 70 bar, permeance and selectivity were nearly constant. Upon attaining 80 bar, a decrease in permeance was detected to $60 \text{ l(STP)}/(\text{m}^2 \cdot \text{h} \cdot \text{bar})$. This reduction was gradual over time and lasted approximately an hour until stable separation parameters were achieved. At the same time, a decline in selectivity from 340 to 240 was noted.

During the subsequent depressurization step, separation parameters were persistent; however, neither the initial value of permeance nor that of selectivity were attained. Such behavior of separation parameters suggests that irreversible changes in the membrane structure occurred at a pressure of 80 bar. The target of further experimental work and analysis was to determine if the change in structure took place in the selective layer or in the support.

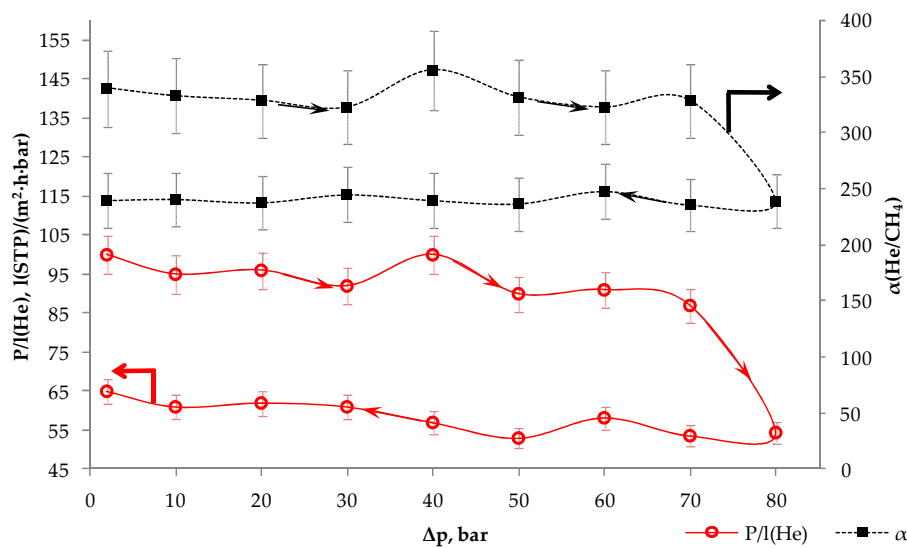


Figure 6. The influence of transmembrane pressure on helium permeance ($P/l(\text{He})$) and selectivity ($\alpha(\text{He}/\text{CH}_4)$) during pressurization and depressurization. The sequence of the experiment is shown by the arrows; lines were drawn to guide the eye.

Certain similarities can be drawn between the aging behavior of thin films and the selective layer of the asymmetric membrane. Upon physical aging of thin films, usually, permeance decreases and selectivity rises slightly or stays on the same level [18–20]. If physical aging of the selective layer occurred, then the decrease in selectivity could be explained by the appearance of new defects. To indicate whether the selective layer was insignificantly damaged, the test ME was subjected to repeated treatment with 0.2% wt. PDMS solution in hexane. An increase in selectivity after treatment would imply that new defects were plugged. In this work, no such increase was observed, which means that the change in separation parameters resulted from the increased support resistance. It is worth noting that significant physical aging was not expected to occur because the fibers were previously annealed at 60 °C.

To estimate the contributions of the selective and support layers to the aging of the membrane, the resistance model by Henis and Tripodi [25] was employed. According to this model, these layers are considered as two separate resistances in series, and a total resistance of the membrane to gas permeation (R_t) can be found using Equation (4).

$$R_t = R_1 + R_2. \quad (4)$$

In this equation, the resistance R represents the ratio of the layer thickness l of the selective layer (1) or the sublayer (2) to the corresponding permeability P_1 or P_2 , respectively. Thus, Equation (4) can be rewritten as

$$\frac{l_t}{P_t} = \frac{l_1}{P_1} + \frac{l_2}{P_2}. \quad (5)$$

The obtained experimental data for $(P/l(\text{He}))_t$, $(P/l(\text{CH}_4))_t$, and $\alpha(\text{He}/\text{CH}_4)_t$ were used to calculate the permeances of the selective and support layers for aged and non-aged hollow fibers (Table 2). According to Knudsen diffusion, the ratio of helium to methane permeances is equal to the inverse ratio of their molecular weights: $\alpha_{\text{KN}}(\text{He}/\text{CH}_4) = 2$. According to the Hagen–Poiseuille model, the selectivity is proportional to the ratio of gas viscosities, approximately 1.8. The real value of the support selectivity is between 1.8 and 2, because it is likely that the transport mechanism in the support layer is transitional between the Knudsen and Hagen–Poiseuille models. In terms of calculation, the change in support selectivity will only slightly affect support permeance values. For the calculations, presented in Table 2, it was assumed that the support layer gas transport

mechanism obeyed Knudsen diffusion. The influence of the PDMS sealing layer was neglected. Intrinsic polymer properties, $P_1(\text{He})$ and $P_1(\text{CH}_4)$ [11], were used to solve Equation (5) for helium and methane permeances and for the calculation of the effective selective-layer thickness.

Table 2. Permeances of selective and support layers, for aged and non-aged hollow fibers, calculated using resistance models.

Parameter	Before Aging	After Aging
$P/l(\text{He})_t, l(\text{STP})/(\text{m}^2 \cdot \text{h} \cdot \text{bar})$	100	60
$P/l(\text{CH}_4)_t, l(\text{STP})/(\text{m}^2 \cdot \text{h} \cdot \text{bar})$	0.29	0.25
$\alpha(\text{He}/\text{CH}_4)_t$	340	240
$P/l(\text{He})_1, l(\text{STP})/(\text{m}^2 \cdot \text{h} \cdot \text{bar})$	144.38	123.03
$P/l(\text{CH}_4)_1, l(\text{STP})/(\text{m}^2 \cdot \text{h} \cdot \text{bar})$	0.29	0.25
Effective selective-layer thickness, nm	82.3	96.6
$P/l(\text{He})_2, l(\text{STP})/(\text{m}^2 \cdot \text{h} \cdot \text{bar})$	325.33	117.12
$P/l(\text{CH}_4)_2, l(\text{STP})/(\text{m}^2 \cdot \text{h} \cdot \text{bar})$	162.67	58.56

The effective selective-layer thickness of the non-aged membrane was 82.3 nm, which agrees well with the SEM micrographs and the “slow” gas permeance measurements presented above. Values of selective and support layer helium permeances were the same order of magnitude, whereas, for methane, the permeance of the support was three orders greater than that of the selective layer. Hence, the observed selectivity was lower than the intrinsic properties due to the support resistance.

After aging, the effective selective-layer thickness, calculated from permeance, increased to 96.6 nm, which suggests that aging of the selective layer occurred. For the aged membrane, selective- and support-layer helium permeance values were almost equal, whereas the resistance of the support to methane permeation could still be neglected compared to the selective layer.

From the calculations in Table 2, it can be seen that both the selective layer and the support layer underwent aging. The effective selective-layer thickness increased by 17%, whereas the support-layer resistance to helium transport displayed a 2.8-fold increase.

To reveal the influence of the support irreversible compaction on the membrane structure, the inner and outer diameters and the porosity of hollow fibers after aging at 80 bar were measured. No significant difference within the margin of error was observed for aged samples compared to the fresh ones, whether in diameter or in porosity.

SEM micrographs of the aged hollow fiber cross-section are presented in Figure 7a,b. Although no noticeable differences were observed between the SEM micrographs of fresh (Figure 4a,b) and aged (Figure 7b) fibers in the vicinity of the selective layer, caution should be taken during such a comparison, because the objects which were studied are near the lower limit of the measurement range. Moreover, the experimental procedure includes soaking in ethanol with subsequent freeze-fracturing in liquid nitrogen, which may slightly change the interspacing between the aggregates.

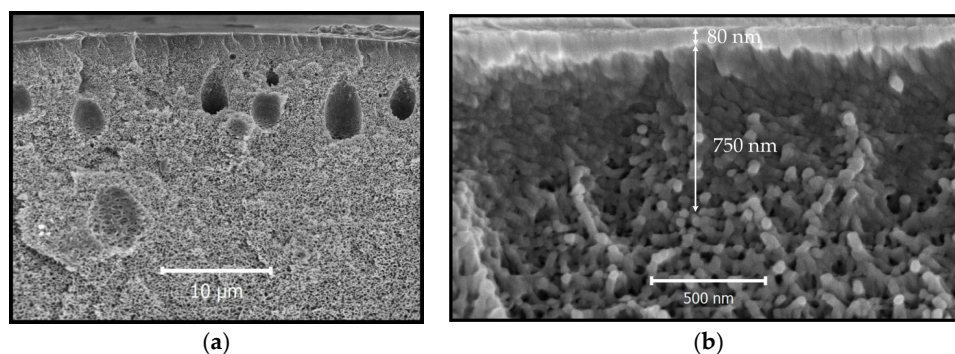


Figure 7. SEM micrographs of the aged hollow fiber cross-section with close-ups of (a) the wall, and (b) the selective layer.

Macrovoids were the first pores expected to contract during high-pressure exposure; however, they were present on the micrograph of the aged fiber (Figure 7a). This suggests that the compaction occurred not in the largest pores of the support, as one would expect, but rather, in the smaller pores. Such pores were present in the transition layer under the skin layer (Figure 4a,b and Figure 7b). They formed a “gutter” layer for the channeling of penetrant molecules from the selective layer to the larger pores of the support.

Low-temperature nitrogen adsorption was employed to examine the influence of aging on the structure of the transitional layer. The pore size distributions for the aged and non-aged samples are presented in Figure 8. It can be noted that the aged sample had a reduced fraction of pores with a radius of less than 15 nm.

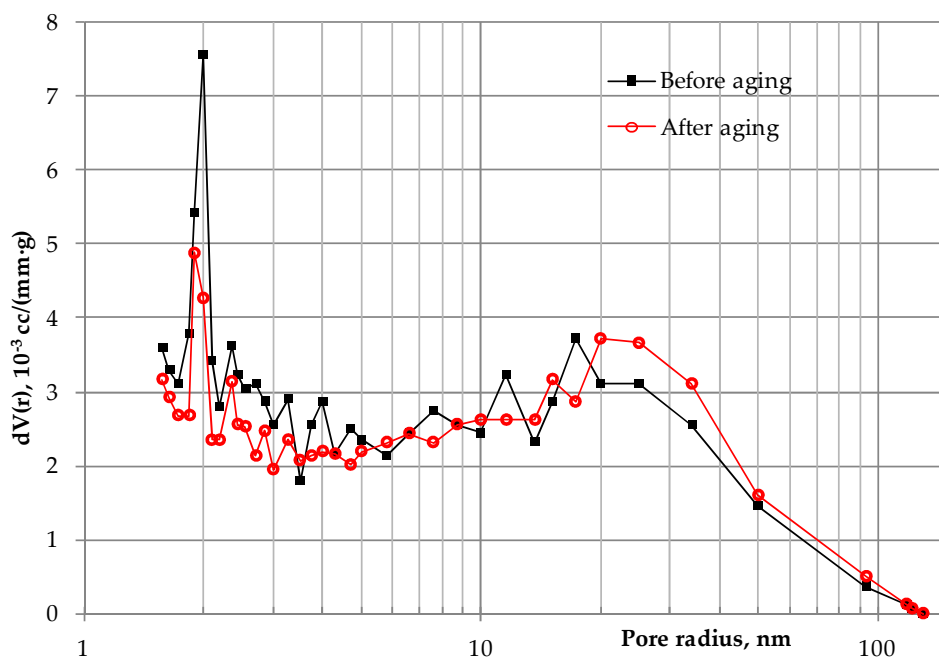


Figure 8. Pore size distribution of hollow fibers before and after aging.

Because the thickness of the transition layer is on the order of several microns, its partial contraction would neither affect the macroscopic geometrical characteristics nor could it be observed on the SEM micrograph of the aged sample. Even a partial contraction of this thin channeling layer would cause a more significant transport resistance for “fast” helium, compared to “slow” methane, which explains the decrease in selectivity [11,25,32].

It is worth noting that big pores and macrovoids contract when exceeding the critical pressure, which is determined from the mechanical properties of the polymer and the structure of the fiber. Usually, this shrinkage is accompanied by a total collapse of the fiber into a thin stripe. Apparently, the mechanism responsible for the contraction of nanopores is different. This is just a hypothesis yet to be proven; however, it may be connected to the strong intermolecular forces of polymer chains. These forces may induce partial “sintering” of polymer aggregates, which are brought closer together upon the application of elevated pressure and temperature.

Values of feed flow rate (q_f), helium concentration in permeate (y_p), and stage cut (θ), which were measured during the pressure increase from 40 to 80 bar in mixed-gas tests and were used to calculate the permeance and selectivity applying the counter-current mathematical model (Figure 6), are presented in Table 3. These values are presented to draw up the material balance or to evaluate the technical and economic performance. The best separation performance, specifically the highest flow rate and helium permeate concentration, and the lowest stage cut, was achieved at 70 bar.

Table 3. The influence of transmembrane pressure on feed flow rate (q_f), helium concentration in permeate (y_p), stage cut (θ), and separation characteristics.

Δp , bar	q_f , 10^{-3} m ³ (STP)/h	y_p (He), %	θ , %	$P/l(\text{He})$, l(STP)/(m ² ·h·bar)	$\alpha(\text{He}/\text{CH}_4)$
40	66	10.6	3.3	100	356
50	93	12.1	2.9	90	332
60	130	13.4	2.6	91	323
70	160	14.7	2.4	87	329
80	150	14.1	2.5	55	239

4. Conclusions

In the current work, a technique was described for obtaining an asymmetric hollow-fiber membrane element with an active membrane area of 0.177 m² from commercial polyamide-imide Torlon® with a helium permeance value of 100 l(STP)/(m²·h·bar) at a selectivity $\alpha(\text{He}/\text{CH}_4)$ of 340. According to the gas permeance test and calculations using resistance models, the skin-layer thickness was 82.3 nm, which was confirmed by SEM micrographs.

The separation performance of this membrane element was investigated in the process of helium extraction from its binary mixture with methane. The complex aging behavior of asymmetric hollow fibers from PAI under elevated pressure (80 bar) was also studied. Aging was accompanied by a decrease in permeance to 60 l(STP)/(m²·h·bar) and in selectivity to 240. Calculations using resistance models showed that both the selective layer and the support layer underwent aging. The effective selective-layer thickness increased by 17%, whereas the support-layer resistance to helium transport displayed a 2.8-fold increase.

To examine the drastic increase in support resistance, the hollow-fiber porous structure was studied. Interestingly, no change was observed in the inner and outer diameters and the porosity. At the same time, a noticeable reduction was observed for the fraction of pores with radii less than 15 nm. SEM micrographs revealed that such pores were located in the transition layer right under the skin layer. This explains why the increase in support resistance was not accompanied by a change in macroscopic characteristics.

Author Contributions: Conceptualization, investigation, methodology, and writing—original draft, review, and editing, G.D. Investigation and methodology, M.I., M.S. and V.S. Supervision, G.K.

Funding: This research received no external funding.

Acknowledgments: The Torlon® 4000T sample was kindly provided by Zakhar Kagramanov (Solvay); the authors thank Andrey Loyko for fruitful discussions and inspiration.

Conflicts of Interest: The authors declare no conflicts of interest.

References

- Bowe, D.J. Helium Recovery and Recycling Makes Good Business Sense. *Ind. Heat.* **2004**, *71*, 79–81.
- Scholes, C.; Stevens, G.; Kentish, S. Membrane gas separation applications in natural gas processing. *Fuel* **2012**, *96*, 15–28. [[CrossRef](#)]
- Häussinger, P.; Glatthaar, R.; Rhode, W.; Kick, H.; Benkmann, C.; Weber, J.; Wunschel, H.-J.; Stenke, V.; Leicht, E.; Stenger, H. Noble gases. 4.2.1.2. Crude Helium Extraction by Permeation Processes. In *Ullmann's Encyclopedia of Industrial Chemistry*, 7th ed.; Walter, G., Ed.; Wiley-VCH: Weinheim, Baden-Württemberg, Germany, 2011; Volume 27, pp. 391–448, ISBN 978-3-527-32943-4.
- Stern, S.A.; Sinclair, T.F.; Gareis, P.J.; Vahldieck, N.P.; Mohr, P.H. Helium recovery by permeation. *Ind. Eng. Chem.* **1965**, *57*, 49–60. [[CrossRef](#)]
- Spillman, R. Economics of Gas Separation Membrane Processes. In *Membrane Separations Technology*; Noble, R., Stern, S., Eds.; Elsevier Science: Eastbourne, UK, 1995; pp. 589–667, ISBN 978-0-444-81633-7.
- Laguntsov, N.I.; Kurchatov, I.M.; Karaseva, M.D.; Solomahin, V.I. On the use of membrane technology for helium extraction from high-pressure natural gas. *Pet. Chem.* **2014**, *54*, 673–679. [[CrossRef](#)]

7. Teplyakov, V.V.; Khotimskii, V.S.; Yakovlev, A.V.; Shalygin, M.G.; Gasanova, L.G.; Zen'kevich, V.B.; Netrusov, A.I. Membrane Systems for the Recovery of Energy Carriers from Products of Organic Waste Recycling. *Catal. Ind.* **2011**, *3*, 62–69. [[CrossRef](#)]
8. Rufford, T.E.; Chan, K.I.; Huang, S.H.; May, E.F. A review of conventional and emerging process technologies for the recovery of helium from natural gas. *Adsorpt. Sci. Technol.* **2014**, *32*, 49–72. [[CrossRef](#)]
9. Sunarso, J.; Hashim, S.S.; Lin, Y.S.; Liuc, S.M. Membranes for helium recovery: An overview on the context, materials and future directions. *Sep. Purif. Technol.* **2016**, *176*, 335–383. [[CrossRef](#)]
10. Scholes, C.A.; Ghosh, U.K. Review of membranes for helium separation and purification. *Membranes* **2017**, *7*, 9. [[CrossRef](#)] [[PubMed](#)]
11. Kosuri, M.R.; Koros, W.J. Defect-free asymmetric hollow fiber membranes from Torlon[®], a polyamide-imide polymer, for high-pressure CO₂ separations. *J. Membr. Sci.* **2009**, *326*, 608–617. [[CrossRef](#)]
12. Peng, N.; Chung, T.S. The effects of spinneret dimension and hollow fiber dimension on gas separation performance of ultra-thin defect-free Torlon[®] hollow fiber membranes. *J. Membr. Sci.* **2008**, *310*, 455–465. [[CrossRef](#)]
13. Peng, N.; Chung, T.S.; Lai, J.Y. The role of additives on dope rheology and membrane formation of defect-free Torlon[®] hollow fibers for gas separation. *J. Membr. Sci.* **2009**, *343*, 62–67. [[CrossRef](#)]
14. Peng, N.; Chung, T.S.; Lai, J.Y. The rheology of Torlon[®] solutions and its role in the formation of ultra-thin defect-free Torlon[®] hollow fiber membranes for gas separation. *J. Membr. Sci.* **2009**, *326*, 608–617. [[CrossRef](#)]
15. Bernardo, P.; Bazzarelli, E.; Tasselli, F.; Clarizia, G.; Mason, C.R.; Maynard-Atem, L.; Budd, P.M.; Lanc, M.; Pilnacek, K.; Vopicka, O.; et al. Effect of physical aging on the gas transport and sorption in PIM-1 membranes. *Polymer* **2017**, *113*, 283–294. [[CrossRef](#)]
16. Swaidan, R.; Ghanem, B.; Litwiller, E.; Pinnau, I. Physical Aging, Plasticization and Their Effects on Gas Permeation in “Rigid” Polymers of Intrinsic Microporosity. *Macromolecules* **2015**, *48*, 6553–6561. [[CrossRef](#)]
17. Dibrov, G.A.; Volkov, V.V.; Vasilevsky, V.P.; Shutova, A.A.; Bazhenov, S.D.; Khotimsky, V.S.; van de Runstraat, A.; Goetheer, E.L.V.; Volkov, A.V. Robust high-permeance PTMSP composite membranes for CO₂ membrane gas desorption at elevated temperatures and pressure. *J. Membr. Sci.* **2014**, *470*, 439–450. [[CrossRef](#)]
18. Rowe, B.W.; Freeman, B.D.; Paul, D.R. Physical aging of ultrathin glassy polymer films tracked by gas permeability. *Polymer* **2009**, *50*, 5565–5575. [[CrossRef](#)]
19. Horn, N.R.; Paul, D.R. Carbon dioxide sorption and plasticization of thin glassy polymer films tracked by optical methods. *Macromolecules* **2012**, *45*, 2820–2834. [[CrossRef](#)]
20. Bakhtin, D.S.; Kulikov, L.A.; Legkov, S.A.; Khotimskiy, V.S.; Levin, I.S.; Borisov, I.L.; Maksimov, A.L.; Volkov, V.V.; Karakhanov, E.A.; Volkov, A.V. Aging of thin-film composite membranes based on PTMSP loaded with porous aromatic frameworks. *J. Membr. Sci.* **2018**, *554*, 211–220. [[CrossRef](#)]
21. Escorihuela, S.; Tena, A.; Shishatskiy, S.; Escolástico, S.; Brinkmann, T.; Serra, J.M.; Abetz, V. Gas Separation Properties of Polyimide Thin Films on Ceramic Supports for High Temperature Applications. *Membranes* **2018**, *8*, 16. [[CrossRef](#)] [[PubMed](#)]
22. Ivanov, M.V.; Storozhuk, I.P.; Dibrov, G.A.; Semyashkin, M.P.; Pavlukovich, N.G.; Kagramanov, G.G. Elaboration of hollow fiber membrane from polyarylate-polyarylate block-copolymer for air separation. *Pet. Chem.* **2018**, *8*, 85–92. [[CrossRef](#)]
23. Ivanov, M.V.; Dibrov, G.A.; Loyko, A.V.; Varezhkin, A.V.; Kagramanov, G.G. Techniques to Manage Geometry Characteristics of Hollow Fiber Membranes. *Theor. Found. Chem. Eng.* **2016**, *50*, 316–324. [[CrossRef](#)]
24. Roy, S.; Singha, N.R. Polymeric Nanocomposite Membranes for Next Generation Pervaporation Process: Strategies, Challenges and Future Prospects. *Membranes* **2017**, *7*, 53. [[CrossRef](#)] [[PubMed](#)]
25. Henis, J.M.S.; Tripodi, M.K. Composite Hollow Fiber Membranes for Gas Separation: The Resistance Model Approach. *J. Membr. Sci.* **1981**, *8*, 233–246. [[CrossRef](#)]
26. Grushevenko, E.A.; Borisov, I.L.; Bakhtin, D.S.; Legkov, S.A.; Bondarenko, G.N.; Volkov, A.V. Membrane material based on octyl-substituted polymethylsiloxane for separation of C₃/C₁ hydrocarbons. *Pet. Chem.* **2017**, *57*, 334–340. [[CrossRef](#)]
27. Grushevenko, E.A.; Podtynnikov, I.A.; Golubev, G.S.; Volkov, V.V.; Borisov, I.L. Polyheptylmethylsiloxane—A novel material for removal of oxygenates from water by pervaporation. *Pet. Chem.* **2018**, *58*, 941–948. [[CrossRef](#)]

28. Pan, C.Y. Gas Separation by Permeators with High-Flux Asymmetric Membranes. *AIChE J.* **1983**, *29*, 545–552. [[CrossRef](#)]
29. Davis, R.; Sandall, O. A Simple Analysis for Gas Separation Membrane Experiments. *Chem. Eng. Educ.* **2003**, *37*, 74–80.
30. Borisov, I.; Ovcharova, A.; Bakhtin, D.; Bazhenov, S.; Volkov, A.; Ibragimov, R.; Gallyamov, R.; Bondarenko, G.; Mozhchil, R.; Bildyukevich, A.; et al. Development of Polysulfone Hollow Fiber Porous Supports for High Flux Composite Membranes: Air Plasma and Piranha Etching. *Fibers* **2017**, *5*, 6. [[CrossRef](#)]
31. Volkov, V.V.; Bildyukevich, A.V.; Dibrov, G.A.; Usoskiy, V.V.; Kasperchik, V.P.; Vasilevsk, V.P.; Novitsky, E.G. Elaboration of Composite Hollow Fiber Membranes with Selective Layer from Poly [1-(trimethylsilyl)-1-propyne] for Regeneration of Aqueous Alkanolamine Solutions. *Pet. Chem.* **2013**, *53*, 619–626. [[CrossRef](#)]
32. Bauer, C.J.M.; Smid, J.; Olijslager, J. The resistance towards gas transport of the sublayer of asymmetric PPO hollow fiber membranes determined by plasmaetching. *J. Membr. Sci.* **1991**, *57*, 307–320. [[CrossRef](#)]
33. Bazhenov, S.D.; Bildyukevich, A.V.; Volkov, A.V. Gas-Liquid Hollow Fiber Membrane Contactors for Different Applications. *Fibers* **2018**, *6*, 76. [[CrossRef](#)]
34. Chung, T.; Kafchinski, R. The effects of spinning conditions on asymmetric 6FDA/6FDAM polyimide hollow fibers for air separation. *J. Appl. Polym. Sci.* **1998**, *65*, 1555–1569. [[CrossRef](#)]
35. Wang, X.; Zhang, L.; Sun, D.; An, Q.; Chen, H. Effect of coagulation bath temperature on formation mechanism of poly(vinylidene fluoride) membrane. *J. Appl. Polym. Sci.* **2008**, *110*, 1656–1663. [[CrossRef](#)]
36. Simone, S.; Galiano, F.; Faccini, M.; Boerrigter, M.E.; Chaumette, C.; Drioli, E.; Figoli, A. Preparation and Characterization of Polymeric-Hybrid PES/TiO₂ Hollow Fiber Membranes for Potential Applications in Water Treatment. *Fibers* **2017**, *5*, 14. [[CrossRef](#)]
37. Peng, N.; Chung, T.-S.; Wang, K.Y. Macrovoid evolution and critical factors to form macrovoid-free hollow fiber membranes. *J. Membr. Sci.* **2008**, *318*, 363–372. [[CrossRef](#)]
38. McKelvey, S.A.; Koros, W.J. Phase separation, vitrification, and the manifestation of macrovoids in polymeric asymmetric membranes. *J. Membr. Sci.* **1996**, *112*, 29–39. [[CrossRef](#)]
39. Scholz, M.; Harlacher, T.; Melin, T.; Wessling, M. Modeling Gas Permeation by Linking Nonideal Effects. *Ind. Eng. Chem. Res.* **2013**, *52*, 1079–1088. [[CrossRef](#)]



© 2018 by the authors. Licensee MDPI, Basel, Switzerland. This article is an open access article distributed under the terms and conditions of the Creative Commons Attribution (CC BY) license (<http://creativecommons.org/licenses/by/4.0/>).